

See discussions, stats, and author profiles for this publication at: <https://www.researchgate.net/publication/280390505>

Charge-Induced Second-Harmonic Generation in Bilayer WSe₂

ARTICLE in NANO LETTERS · JULY 2015

Impact Factor: 13.59 · DOI: 10.1021/acs.nanolett.5b02547 · Source: PubMed

READS

70

5 AUTHORS, INCLUDING:



D. Talukdar

Nanyang Technological University

16 PUBLICATIONS 33 CITATIONS

SEE PROFILE



Weigao Xu

Peking University

11 PUBLICATIONS 357 CITATIONS

SEE PROFILE



Jacob B Khurgin

Johns Hopkins University

577 PUBLICATIONS 5,040 CITATIONS

SEE PROFILE



Qihua Xiong

Nanyang Technological University

166 PUBLICATIONS 3,984 CITATIONS

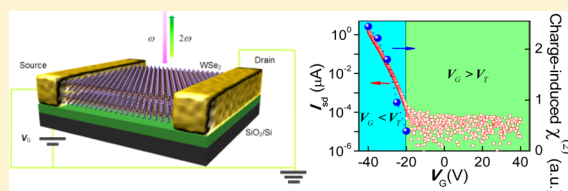
SEE PROFILE

Charge-Induced Second-Harmonic Generation in Bilayer WSe₂Huakang Yu,[†] Deep Talukdar,[†] Weigao Xu,[†] Jacob B. Khurgin,^{*,‡} and Qihua Xiong^{*,†,§}[†]Division of Physics and Applied Physics, School of Physical and Mathematical Sciences, Nanyang Technological University, 637371 Singapore[‡]Department of Electrical and Computer Engineering, Johns Hopkins University, Baltimore, Maryland 21218, United States[§]NOVITAS, Nanoelectronics Centre of Excellence, School of Electrical and Electronic Engineering, Nanyang Technological University, 639798 Singapore

Supporting Information

ABSTRACT: Controlling nonlinear light–matter interaction is important from a fundamental science point of view as well as a basis for future optoelectronic devices. Recent advances in two-dimensional crystals have created opportunities to manipulate nonlinear processes electrically. Here we report a strong second-harmonic generation (SHG) in a 2D WSe₂ bilayer crystal caused by a back gate field. This unusual process takes place only when the gate polarity causes charge accumulation rather than depletion. Analysis based on a bond–charge model traces the origin of SHG to the nonuniform field distribution within a single monolayer, caused by the accumulated submonolayer screening charge in the tungsten plane. We name this phenomenon charge-induced SHG (CHISHG), which is fundamentally different from the field- or current-induced SHG. Our findings provide a potentially valuable technique for understanding and noninvasive probing of charge and current distributions in future low dimensional electronic devices.

KEYWORDS: Charge-induced second-harmonic generation, two-dimensional layered materials, tungsten diselenide, bond charge model, charge accumulation, screening effect



Two-dimensional (2D) atomic materials exhibit extraordinary optical and electronic properties and have been intensively investigated over the past decade or so.^{1,2} With dimensions reduced to a monolayer, exceptional physical behaviors such as indirect–direct bandgap transition and inversion symmetry breaking have been discovered enabling various potential applications in nanoscale electronics and photonics.^{3–6} Especially important is the ability to modulate the physical properties down to quantum size regime by external stimuli as it provides new avenues for exploring physics and technological applications. For instance, electric field and artificial stacking have been recently used for tuning orbital magnetic moment and Berry curvature of the Bloch states in bilayer graphene and 2D transition metal dichalcogenides (TMDs).^{7–10}

In this work we demonstrate manipulation of the bond charges in a bilayer TMD by applying a perpendicular electric field, which causes significant modification of the nonlinear optical properties, manifested by second-harmonic generation (SHG). The key difference between our results and numerous prior works on electric-field-induced SHG (E-FISHG)^{11–17} is that CHISHG is observed only when the applied electric field causes space charge accumulation, which can occur in either accumulation or deep inversion mode of operation but not in the depletion mode. The microscopic origin of the effect can be traced to the specific nature of the electronic states at the direct band edges of 2D TMD¹⁸ that are predominantly composed of the d_{xy} and $d_{x^2-y^2}$ orbitals of transition metal (W) as shown in

Figure 1a and explained in greater detail in the Supporting Information. The accumulation charge is thus highly localized in the transition metal planes (i.e., x – y plane), and the DC field becomes highly nonuniform due to the screening effect, which is fundamentally different from E-FISHG in conventional metal–semiconductor or metal–oxide–semiconductor structures^{12,15–17} where the effect has a macroscopic character. As a result, E-FISHG, nearly forbidden by symmetry in the case of uniform DC field, becomes allowed. Thus, SHG measurement can serve as a gauge of space charge and electric field distribution on a submonolayer scale.

In our experiment, bilayer WSe₂ samples on 100 nm silicon oxide substrate were prepared by mechanical exfoliation method confirmed by Raman spectroscopy, which exhibits characteristic low-frequency shear and breathing modes extremely sensitive to layer numbers in transitional metal dichalcogenides.^{19,20} The pristine WSe₂ layers stacked in 2H order have inversion symmetry, leading to vanishing second-order optical nonlinearity (Figure 1b).^{21–25} Back-gated field-effect transistors (FETs) were fabricated using these flakes in order to investigate the charge-induced SHG (see Methods). Source-drain electrodes remain grounded during the experiments (Figure 1c) for excluding the possibility of current-induced SHG.^{26,27}

Received: June 27, 2015

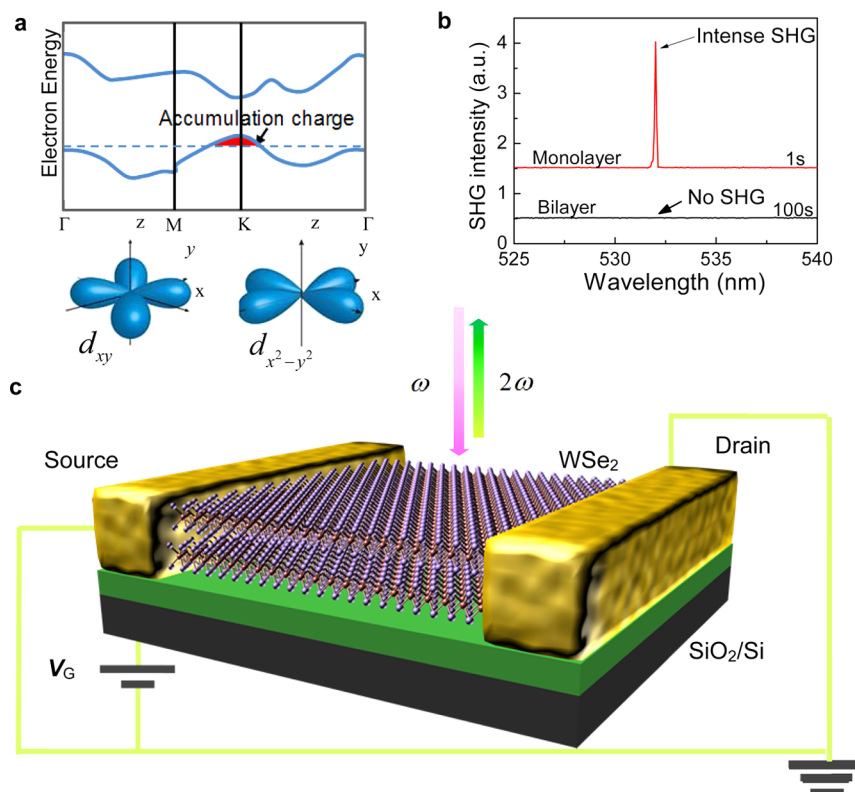


Figure 1. ISHG measurements of back-gated bilayer WSe₂ FET. (a) Schematic energy diagram of monolayer WSe₂. Holes are accumulated (red) under certain back-gate potentials. (b) Typical SHG spectra from monolayer and bilayer WSe₂ samples. The spectra have been shifted vertically for clarity. (c) Schematic diagram of the device configuration of WSe₂ during the SHG experiments.

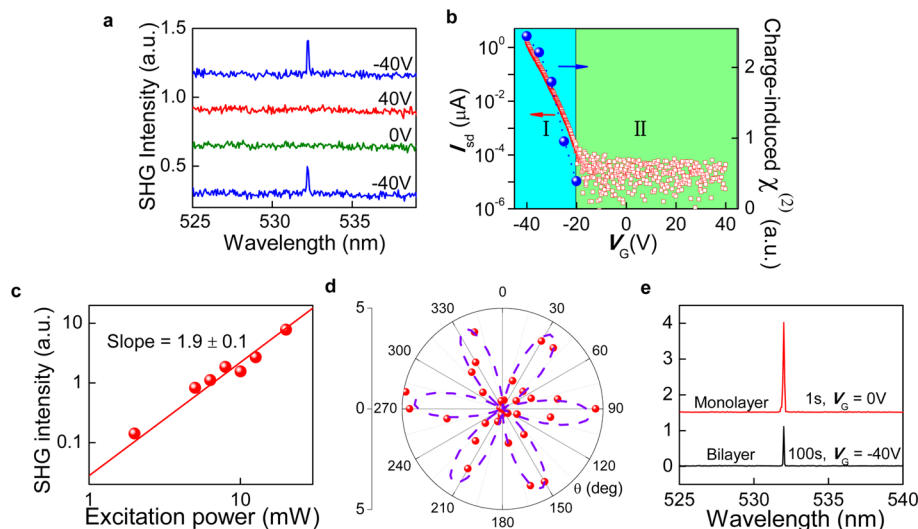


Figure 2. Charge-induced SHG from bilayer WSe₂. (a) Reversible SHG induced by back gate can be seen from the pristine bilayer WSe₂ sample. The spectra have been shifted vertically for clarity. (b) I_{sd} vs V_G curve of the bilayer WSe₂ device. The blue region (I) represents $V_G < V_T$ (hole accumulation) while the green region (II) represents $V_G > V_T$. SHG intensities as a function of gate voltage (blue dots) are superimposed on I_{sd} vs. V_G curve. (c) Log–log plot of power dependence of the CHISHG intensity on the incident laser power at $V_G = -40$ V. The red circles represent the experimental data and the red line represents a linear fit with extracted slope 1.9 ± 0.1 . (d) Polar plot of polarization-resolved CHISHG intensity (red circles) from the bilayer WSe₂ sample at $V_G = -25$ V. The blue line shows the expected $\cos^2(3\theta)$ dependence. (e) Red line shows the SHG intensity recorded from monolayer with detector integration time of 1 s and black line from bilayer at $V_G = -40$ V with integration time of 100 s under the same experimental conditions, respectively. The charge-induced $\chi_{xxx,b}^{(2)}(V)$ is estimated to be around 0.03 of $\chi_{xxx,m}^{(2)}$.

The results of gate-voltage-dependent SHG measurements are shown in Figure 2a. At zero gate bias ($V_G = 0$ V), no SHG signal was detected. Upon the application of a negative gate bias $V_G = -40$ V, there is a charge (hole) accumulation in the

sample and efficient SHG can be observed, as shown by the back-gate sweep of source-drain current I_{sd} (Figure 2b). The obtained transfer characteristics are of typical *p*-type conduction operated in enhancement mode with a turn-on

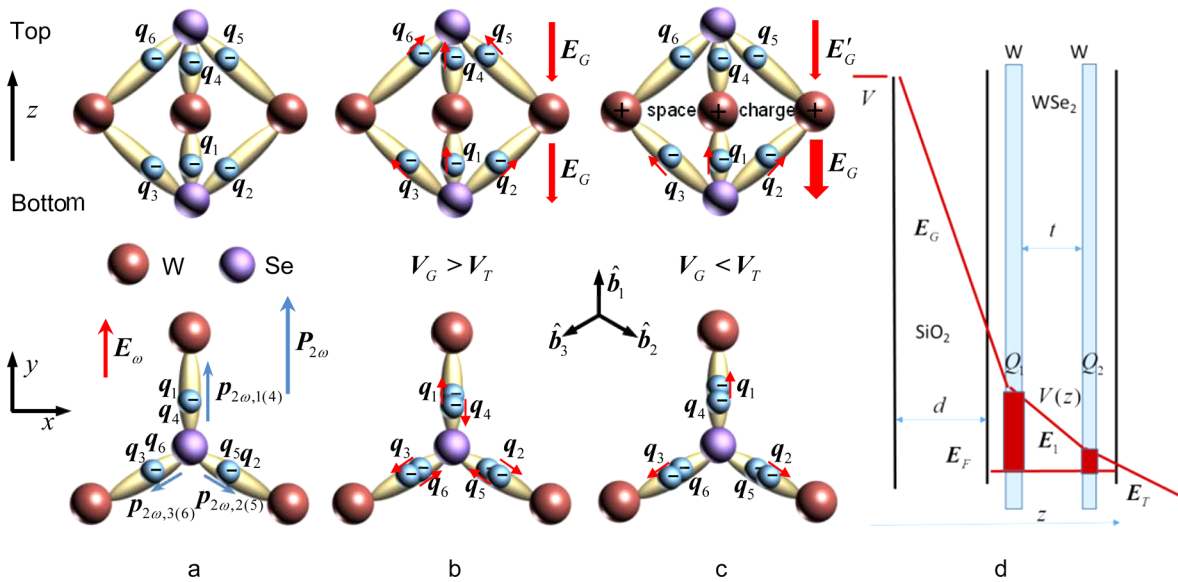


Figure 3. |Bond-charge model upon back-gate fields. (a) Schematic diagram of bond-charge distributions within one WSe₂ unit cell without external electric field, where q_n ($n = 1, 2, 3, 4, 5, 6$) represents the bond charge of each W–Se bond in one unit cell. Insets show the crystallographic axis and Cartesian coordinates. A total $P_{2\omega}$ is generated while applying an in-plane optical field E_ω polarized along the y -direction. (b) Perturbation of bond charges in each W–Se bond while applying a DC gate field E_G (for $V_G > V_T$) in the vertical direction, where the total second-order susceptibility remains unchanged and no E-FISHG is expected. (c) An atomically thin hole-charge sheet is generated while applying E_G (for $V_G < V_T$), which pins the external electric field in the top half-monolayer. This screening effect is responsible for the observed CHISHG. (d) Schematic diagram of the electric field and charge distribution in the WSe₂/SiO₂/Si structure on application of a transverse field (not to scale). For $V_G = -40$ V the electric field is pinned at the threshold field E_T for the top monolayer. The charges are nonuniformly distributed in the adjacent two monolayers due to screening.

threshold voltage $V_T \approx -20$ V. In contrast, switching the polarity, i.e., $V_G = 40$ V, yields no SHG signal. In order to understand the evolution of SHG as a function of gate voltage we plotted the magnitude of the square root of SHG intensity (i.e., relative change of charge-induced second-order susceptibility $\chi^{(2)}$) and superimposed it on $I_{sd} - V_G$ characteristics as shown in Figure 2b, which represents the key result of this work. The charge-induced $\chi^{(2)}$ is zero below threshold and increases linearly after V_T , as the back gate voltage becomes increasingly negative indicating that $\chi^{(2)}$ is proportional to the accumulated charge and thus justifying the term charge-induced SHG (CHISHG). Furthermore, we have performed power-dependent measurements, which revealed a quadratic dependence shown as the log–log plot in Figure 2c, a tell-tale sign of a second-order optical process. The polarization symmetry of CHISHG was also investigated, as shown in Figure 2d. The observed 6-fold symmetry, combined with further confirmation of the angle-independent behavior of total amount of CHISHG, is identical to the one observed in the monolayer with D_{3h} symmetry.²⁴ The intensity of CHISHG signal from bilayer flake at $V_G = -40$ V was about 1000 times less than SHG signal from a monolayer WSe₂ measured under the same experimental conditions (Figure 2e), indicating that $\chi^{(2)}$ was about 30 times less. In order to demonstrate the sufficient sensitivity of CW laser used here, we have successfully reproduced the asymmetric threshold-like behavior in the hole-accumulation regime by using a femtosecond laser excitation (as shown in Supporting Information Section 8).

To explicate these results a bond charge model²⁸ was invoked. In this model potential difference between W and Se ions in each bond \hat{b}_n causes a shift of the position of center of the bond charge q_n relative to the bond center and gives rise to a second-order bond hyperpolarizability $\beta_n^{(2)}$, responsible for the

bulk susceptibility $\chi^{(2)}$.^{29,30} When an in-plane optical field $E_\omega e^{i\omega t}$ is applied as shown in Figure 3a (here we use y direction as an example), second-order dipole moment $p_{2\omega,n} = \beta_n^{(2)}(E_\omega \cdot \hat{b}_n)^2 e^{2i\omega t}$ is generated in each bond. Since the electric field $E_\omega e^{i\omega t}$ makes different angles with each bond \hat{b}_n , the dipoles $p_{2\omega,n}$ have different magnitudes and thus cannot cancel; hence, a nonvanishing monolayer polarization $P_{2\omega} e^{2i\omega t}$ arises. In a more general case, if the electric field $E_\omega e^{i\omega t}$ is directed at an arbitrary angle θ to one of the bonds, nonlinear polarization has an angular dependence, $P_{2\omega} \approx \cos(3\theta)$ considering the trigonal symmetry of the bonds. That is what is observed in a monolayer of WSe₂, but in a bilayer WSe₂, the bonds in the second monolayer have opposite symmetry in the x – y plane with respect to the bonds in the first layer. As a result, nonlinear polarizations of two monolayers cancel and indeed no SHG has been observed in a bilayer (see Figure 1b).

When a gate field V_G is applied, it is natural to expect E-FISHG; yet this is not the case in TMD. As shown in Figure 3b, the perpendicular external electric field leads to upward shift bond charges q_n for all six bonds. However, the hyperpolarizabilities $\beta_{1-3}^{(2)}$ in the bottom half monolayer are reduced as the bond charges in q_{1-3} move toward W ions reducing bond polarities, whereas for the top half-monolayer bond charges in q_{4-6} move toward Se ions increasing hyperpolarizabilities $\beta_{4-6}^{(2)}$. Therefore, on average neither polarity nor hyperpolarizability change, and there is no change of overall $\chi^{(2)}$, which is in accordance with E-FISHG theory considering that there is no third-order susceptibility tensor with out-of-plane element (e.g., $\chi_{xxxz}^{(3)}$). Consequently, no E-FISHG can be observed for as long as the applied DC field is uniform, which is precisely what happens in the absence of accumulation charge.

When the gate voltage exceeds threshold, a hole accumulation layer is formed on the W $5d_{x^2-y^2,xy}$ orbitals (Figure 1a),

and it acts as a screening charge that prevents further field penetration beyond this accumulation plane. Microscopically, reducing V_G beyond threshold compels bond charge to shift further toward W atoms in the bottom half-monolayer while not affecting the top half-monolayer (Figure 3c). This leads to a decrease in $\beta_{1-3}^{(2)}$, which is no longer compensated, and the total $\chi^{(2)}$ of the monolayer changes. For the bilayer described here the effect would have been canceled if a similar shielding charge Q_2 had been accumulated in the second monolayer. However, the density of the band edge states is so high that practically the entire space charge is localized in the W plane of the bottom layer as shown in Figure 3d. As explained in the Supporting Information (section 3), from simple electrostatic considerations the charge Q_2 in the W plane of the top layer is only 4% of the charge Q_1 . Therefore, the field-induced change in $\chi^{(2)}$ of the bottom monolayer remains largely uncompensated resulting in nonvanishing overall $\chi^{(2)}$, proportional to $|V_G - V_T|$. To summarize, it is the charge accumulation that induces SHG, which warrants using the term charge-induced SHG, CHISHG, to describe the phenomenon observed in our experiments. The SHG is possible only in the presence of accumulated charge, which can occur in either accumulation or inversion mode of operation, but not in the depletion mode. This observation is further confirmed by the results for the different WSe₂ sample with ambipolar transport characteristics in which the CHISHG had been observed in the presence of both hole (accumulation mode) and electron (deep inversion mode) accumulation charges with no SHG observed between those two modes (see Figure S4).

To obtain an order-of-magnitude estimate of CHISHG and compare it with experimental results, we use the same simple bond charge model of $\chi^{(2)}$.²⁸ At $V_G = -40$ V the effective gate-induced potential difference between the W and Se layers that causes shift of the bond charges and change of bond hyperpolarizability $\Delta\beta^{(2)}(V)$ is given by $\Delta V_{\text{eff}} = |V - V_T|t'/d_{\text{ox}} \approx 0.03$ V, where $t' = 0.15$ nm is the distance between W and Se layers and $d_{\text{ox}} = 100$ nm is the oxide thickness. This potential augments the existing effective potential difference between W and Se ions, usually referred to as heteropolar contribution to the bandgap C .^{31–33} In a typical nonlinear material GaAs the heteropolar potential is $C_{\text{GaAs}} = 4.3$ eV.³⁴ Second-order susceptibility is proportional to C of bonds, the cube of bond length l_B , and the volume density of bonds N_B .²⁸ It follows that, since both theory and experimental data estimate the magnitudes of $\chi^{(2)}$ of WSe₂ and GaAs are comparable,³⁵ we can estimate heteropolar potential for WSe₂ as $C_{\text{WSe}_2} \approx C_{\text{GaAs}}(l_{B,\text{GaAs}}/l_{B,\text{WSe}_2})^3(N_{B,\text{GaAs}}/N_{B,\text{WSe}_2}) \approx 0.83$ eV, a value that appears to be reasonable in view of lesser ionicity of WSe₂ (see Supporting Information for details). We now relate the charge-induced susceptibility of a bilayer material $\chi_{\text{xxx},b}^{(2)}(V)$ to the susceptibility of one WSe₂ monolayer $\chi_{\text{xxx},m}^{(2)}(V)$ as $\chi_{\text{xxx},b}^{(2)}(V)/\chi_{\text{xxx},m}^{(2)} = \Delta\beta_b^{(2)}(V)/2\beta_b^{(2)} \approx e\Delta V_{\text{eff}}/2C_{\text{WSe}_2} \approx 0.02$ where factor of 1/2 takes into account the fact that only the bottom half-monolayer contributes to SHG in bilayer material. This result is quite close to our experimentally determined ratio of susceptibilities of 0.03 and thus confirms the validity of the model. Another possible contribution by direct charge accumulation via bond polarizability bleaching mechanism is weak and can be excluded (see Supporting Information section 6). It is important to comment that the sharp threshold-like dependence of SHG can be explained only by the microscopic model developed here that takes into consideration underlying

orbital structure but not by the conventional bulk $\chi^{(2)}$ used in refs 15–17. This model also offers an explanation for the observed saturation (reduction in slope) of SHG intensity at large voltages (Figure 2B). Since the energy difference between the direct (K) and indirect (Γ) band-edges (Figure 1A) is only about 100 meV (or less), eventually the accumulation charge spills-over into the Γ band-edge states, such that charge is no longer localized in a plane of W atoms but spread out between W and S atoms; hence, the SHG efficiency growth is no longer proportional to the charge as is the case in Figure 2b. It is also important to note that according to our model CHISHG can occur only in direct bandgap TMDs having band extrema in the K -point of the Brillouin zone, and indeed, when we have tested four-layer WSe₂ samples with an indirect bandgap, no CHISHG had been observed.

In summary, we have demonstrated a fundamentally new nonlinear optical phenomenon, CHISHG in TMDs, and developed a microscopic physical model proving that SHG is engendered by the localized accumulation charge causing DC field nonuniformity. This CHISHG is fundamentally different from a recent work³⁶ on electric field control of the SHG in a monolayer of WSe₂, which was observed only at the exciton resonance and did not show threshold characteristics versus gate voltage. In contrast, in the bilayer of WSe₂ used in our experiments off-resonant (hence free from PL background) SHG has shown threshold and asymmetry behaviors that are unambiguously associated with the presence of mobile charges on the d-shells of W, a unique characteristic of only TMD materials. Our results demonstrate significance of charge and field distribution on the scale of a single atomic layer and should serve as an impetus for potential applications in noninvasive probing of charge and current distributions in future low dimensional electronic devices.

Methods. Bilayer WSe₂ flakes were exfoliated from commercial WSe₂ crystals using scotch-tape method on SiO₂/Si substrates (100 nm SiO₂). Bilayers were identified and confirmed using optical contrast in a microscope followed by atomic force microscopy and low-frequency Raman spectroscopy (see Figure S1). Using electron beam lithography techniques back-gated field-effect transistors (FETs) were fabricated. Electrodes (5 nm/50 nm Ti/Pd) were then deposited on the patterned devices using UHV thermal evaporation followed by hot acetone lift-off. The device performance and gate-dependent transport were then checked in a shielded Lakeshore probe station using an Agilent Parameter Analyzer B1500A. A linearly polarized continuous-wave 1064 nm laser of 30 mW power was focused on the samples via a 100× objective (Leica, HCX PL FLUOTAR L 100×/0.75), and SHG signals were collected in the reflection geometry. A short-pass filter (Semrock, FF01-770/SP-25) was used in front of the spectrometer. SHG signals were then dispersed by a grating of 600 g/mm and recorded by a liquid nitrogen cooled CCD. During the nonlinear optical measurements, a back gate voltage was applied while keeping source-drain electrodes grounded. The sensitivity of experiment was confirmed to be sufficient here by examining the quadratic power dependence of CHISHG. A linear polarizer was used to investigate the anisotropy of polarized SHG while rotating the bilayer samples. The observed 6-fold symmetry indicated the capability of determining the crystal orientation of 2H-stacked bilayer WSe₂ crystals, which was only accessible in odd number layer samples.^{21–25}

■ ASSOCIATED CONTENT

Supporting Information

The Supporting Information is available free of charge on the ACS Publications website at DOI: 10.1021/acs.nanolett.5b02547.

Additional information regarding device fabrication, characterization, polarization-dependent SHG intensity, bond-charge model analysis, and CHISHG by a femto-second laser (PDF)

■ AUTHOR INFORMATION

Corresponding Authors

*E-mail: qihua@ntu.edu.sg.

*E-mail: jakek@jhu.edu.

Author Contributions

H.K.Y. and Q.X. conceived the idea; Q.X. and J.B.K. supervised the project; H.K.Y., D.T., and W.G.X. fabricated the devices and performed the experiments; H.K.Y., J.B.K., and Q.X. analyzed the data and cowrote the manuscript. All the authors commented on the manuscript.

Notes

The authors declare no competing financial interest.

■ ACKNOWLEDGMENTS

Q.X. gratefully acknowledges the strong support of this work from Singapore National Research Foundation through a Fellowship award (NRF-RF2009-06) and an Investigatorship award (NRF-NRFI2015-03). This work was also supported in part by Singapore Ministry of Education via two Tier 2 grants (MOE2011-T2-2-051 and MOE2012-T2-2-086) and start-up grant support (M58113004) from Nanyang Technological University (NTU). J.B.K. is pleased to acknowledge support from NSF DMR-1207245 grant.

■ REFERENCES

- (1) Geim, A. K.; Novoselov, K. S. The rise of graphene. *Nat. Mater.* **2007**, *6*, 183–191.
- (2) Wang, Q. H.; Kalantar-Zadeh, K.; Kis, A.; Coleman, J. N.; Strano, M. S. Electronics and optoelectronics of two-dimensional transition metal dichalcogenides. *Nat. Nanotechnol.* **2012**, *7*, 699–712.
- (3) Mak, K. F.; Lee, C.; Hone, J.; Shan, J.; Heinz, T. F. Atomically thin MoS₂: a new direct-gap semiconductor. *Phys. Rev. Lett.* **2010**, *105*, 136805.
- (4) Splendiani, A.; et al. Emerging photoluminescence in monolayer MoS₂. *Nano Lett.* **2010**, *10*, 1271–1275.
- (5) Liu, L.; Bala Kumar, S.; Ouyang, Y.; Guo, J. Performance limits of monolayer transition metal dichalcogenide transistors. *IEEE Trans. Electron Devices* **2011**, *58*, 3042–3047.
- (6) Zhao, W.; et al. Origin of Indirect Optical Transitions in Few-Layer MoS₂, WS₂, and WSe₂. *Nano Lett.* **2013**, *13*, 5627–5634.
- (7) Zhang, Y.; et al. Direct observation of a widely tunable bandgap in bilayer graphene. *Nature* **2009**, *459*, 820–823.
- (8) Mak, K. F.; Lui, C. H.; Shan, J.; Heinz, T. F. Observation of an electric-field-induced band gap in bilayer graphene by infrared spectroscopy. *Phys. Rev. Lett.* **2009**, *102*, 256405.
- (9) Wu, S.; et al. Electrical tuning of valley magnetic moment through symmetry control in bilayer MoS₂. *Nat. Phys.* **2013**, *9*, 149–153.
- (10) Jiang, T.; et al. Valley and band structure engineering of folded MoS₂ bilayers. *Nat. Nanotechnol.* **2014**, *9*, 825–829.
- (11) Terhune, R.; Maker, P.; Savage, C. Optical harmonic generation in calcite. *Phys. Rev. Lett.* **1962**, *8*, 404.
- (12) Lee, C.; Chang, R.; Bloembergen, N. Nonlinear electro-reflectance in silicon and silver. *Phys. Rev. Lett.* **1967**, *18*, 167.

- (13) Hsieh, D.; et al. Nonlinear Optical Probe of Tunable Surface Electrons on a Topological Insulator. *Phys. Rev. Lett.* **2011**, *106*, 057401.
- (14) Cai, W.; Vasudev, A. P.; Brongersma, M. L. Electrically controlled nonlinear generation of light with plasmonics. *Science* **2011**, *333*, 1720–1723.
- (15) Aktsipetrov, O.; et al. dc-electric-field-induced second-harmonic generation in Si (111)-SiO₂-Cr metal-oxide-semiconductor structures. *Phys. Rev. B: Condens. Matter Mater. Phys.* **1996**, *54*, 1825.
- (16) Ohlhoff, C.; Lüpke, G.; Meyer, C.; Kurz, H. Static and high-frequency electric fields in silicon MOS and MS structures probed by optical second-harmonic generation. *Phys. Rev. B: Condens. Matter Mater. Phys.* **1997**, *55*, 4596.
- (17) Aktsipetrov, O.; et al. dc-electric-field-induced and low-frequency electromodulation second-harmonic generation spectroscopy of Si (001)-SiO₂ interfaces. *Phys. Rev. B: Condens. Matter Mater. Phys.* **1999**, *60*, 8924.
- (18) Finteis, T.; et al. Occupied and unoccupied electronic band structure of WSe₂. *Phys. Rev. B: Condens. Matter Mater. Phys.* **1997**, *55*, 10400.
- (19) Zhao, Y.; et al. Interlayer breathing and shear modes in few-layer MoS₂ and WSe₂. *Nano Lett.* **2013**, *13*, 1007–1015.
- (20) Luo, X.; et al. Effects of lower symmetry and dimensionality on Raman spectra in two-dimensional WSe₂. *Phys. Rev. B: Condens. Matter Mater. Phys.* **2013**, *88*, 195313.
- (21) Malard, L. M.; Alencar, T. V.; Barboza, A. P. M.; Mak, K. F.; de Paula, A. M. Observation of intense second harmonic generation from MoS₂ atomic crystals. *Phys. Rev. B: Condens. Matter Mater. Phys.* **2013**, *87*, 201401.
- (22) Zeng, H.; et al. Optical signature of symmetry variations and spin-valley coupling in atomically thin tungsten dichalcogenides. *Sci. Rep.* **2013**, *3*, 1608.
- (23) Kumar, N.; et al. Second harmonic microscopy of monolayer MoS₂. *Phys. Rev. B: Condens. Matter Mater. Phys.* **2013**, *87*, 161403.
- (24) Li, Y.; et al. Probing symmetry properties of few-layer MoS₂ and h-BN by optical second-harmonic generation. *Nano Lett.* **2013**, *13*, 3329–3333.
- (25) Yin, X. B.; et al. Edge Nonlinear Optics on a MoS₂ Atomic Monolayer. *Science* **2014**, *344*, 488–490.
- (26) Khurgin, J. B. Current induced second harmonic generation in semiconductors. *Appl. Phys. Lett.* **1995**, *67*, 1113–1115.
- (27) Ruzicka, B. A.; et al. Second-harmonic generation induced by electric currents in GaAs. *Phys. Rev. Lett.* **2012**, *108*, 077403.
- (28) Levine, B. Bond-charge calculation of nonlinear optical susceptibilities for various crystal structures. *Phys. Rev. B* **1973**, *7*, 2600.
- (29) Shen, Y. R. *The Principles of Nonlinear Optics*; Wiley-Interscience: New York, 1984.
- (30) Boyd, R. W. *Nonlinear Optics*; Academic Press: New York, 2003.
- (31) Phillips, J. Dielectric definition of electronegativity. *Phys. Rev. Lett.* **1968**, *20*, 550.
- (32) Van Vechten, J. A. Quantum dielectric theory of electronegativity in covalent systems. I. Electronic dielectric constant. *Phys. Rev.* **1969**, *182*, 891.
- (33) Van Vechten, J. Quantum dielectric theory of electronegativity in covalent systems. II. Ionization potentials and interband transition energies. *Phys. Rev.* **1969**, *187*, 1007.
- (34) Christensen, N.; Satpathy, S.; Pawłowska, Z. Bonding and ionicity in semiconductors. *Phys. Rev. B: Condens. Matter Mater. Phys.* **1987**, *36*, 1032.
- (35) Wang, C. Y.; Guo, G. Y. Nonlinear Optical Properties of Transition Metal Dichalcogenide MX₂ (M= Mo, W; X= S, Se) Monolayers and Trilayers from First-principles Calculations. *J. Phys. Chem. C* **2015**, *119*, 13268.
- (36) Seyler, K. L.; et al. Electrical control of second-harmonic generation in a WSe₂ monolayer transistor. *Nat. Nanotechnol.* **2015**, *10*, 407–411.